Quanta Image Sensor: Concepts and Progress

Invited Paper

Eric R. Fossum[1], Jiaju Ma, and Saleh Masoodian
Thayer School of Engineering at Dartmouth
Dartmouth College, Hanover, NH USA 03755

ABSTRACT

The QIS was conceived when contemplating shrinking pixel sizes and storage capacities, and the steady increase in digital processing power. In the single-bit QIS, the output of each field is a binary bit plane, where each bit represents the presence or absence of at least one photoelectron in a photodetector. A series of bit planes is generated through high-speed readout, and a kernel or "cubicle" of bits (x,y,t) is used to create a single output image pixel. The size of the cubicle can be adjusted post-acquisition to optimize image quality. The specialized sub-diffraction-limit photodetectors in the QIS are referred to as "jots" and a QIS may have a gigajot or more, read out at 1000 fps, for a data rate exceeding 1Tb/s. Basically, we are trying to count photons as they arrive at the sensor. This paper reviews the Quanta Image Sensor (QIS) concept and its imaging characteristics. Recent progress towards realizing the QIS for commercial and scientific purposes is discussed. The QIS represents a possible major paradigm shift in image capture.

Keywords: Photon counting, image sensor, quanta image sensor, QIS, low read noise, low power.

1. INTRODUCTION

The Quanta Image Sensor (QIS) was conceived in 2004 [1-4] as a forward look at where image sensors may go in the 10 to 15-year future as progress in semiconductor device technology would allow sub-diffraction limit (SDL) pixels to be readily implemented, and advancement in circuit design and scaling would permit greater pixel throughput at reasonable power dissipation levels. Active research began in 2008 at Samsung [5] but was short lived due to economic pressure in that period. Research began anew at Dartmouth in 2011 and was supported from 2012 to the present by Rambus, Inc. Since then, progress has been made in pixels, readout circuits, and image formation [6-26]. In this paper, the QIS concept and progress to date is reviewed.

In the QIS, SDL pixels (e.g. 200nm-1000nm pitch) are sensitive to single photoelectrons, so that the presence or absence of one electron will result in a logical binary output of 0 or 1 upon readout. The specialized pixel, called a "jot," (Greek for "smallest thing") needs only the smallest full-well capacity (FWC). It is envisioned that a QIS will consist of hundreds of millions or perhaps billions of jots read out at perhaps 1000 fields per second, resulting in a series of bit planes, each corresponding to one field. The bit data can be thought of as a jot data cube, with two spatial dimensions (x and y) with the third dimension being time.

Output image pixels are created by locally processing the jot data cube to create a representation of local light intensity received by the QIS. Since this processing occurs post-capture, great flexibility is afforded in choosing the effective spatial dimensions of a pixel as well as its temporal dimension (e.g., integration time). Conceptually, if the bit data is an accurate representation of the collection and counting of photoelectrons, the combining of jot data is noiseless, allowing functionality such as time-delay-and-integration (TDI) to be performed post-capture on the data in an arbitrary track direction. In fact, different tracks can be used in different portions of the image. Indeed, even relative motion of objects within the field of view can be determined and refined iteratively to optimize the image generation process. Spatial and temporal resolution can also be adjusted for different portions of the image.

Possible applications of the QIS include scientific low-light imaging such as in life sciences (e.g. microscopy), defense and aerospace, professional and consumer photography and cinematography, multi-aperture imaging, cryptography (quantum random number generation), direct detection of low-energy charged particles, and others.

[1] eric.r.fossum@dartmouth.edu http://engineering.dartmouth.edu/people/faculty/eric-fossum/

To appear in *Advanced Photon Counting Techniques X*, Proc. SPIE Vol. 9858, paper 4, April 20-21, Baltimore, MD USA (2016).

To realize the QIS in a convenient form, several theoretical and technological issues required exploration. These are (1) image formation algorithms that yield high quality images, (2) understanding the imaging characteristics of QIS devices, (3) the implementation of pixels (jots) that enable photon counting, (4) low-power readout of high volumes of data (readout of a 1Gjot sensor at 1000fps yields a data throughput rate of 1Tb/s) and (5) on-focal-plane processing to reduce the data volume. Exploration of these issues of the course of the last several years has led to significant advancement in the first four areas with the fifth just being explored now. This paper is a condensed version of a longer paper that reviews that progress [27].

2. CREATING IMAGES FROM JOTS

Readout of jots results in a bit cube of data (see Fig. 1), with two dimensions representing spatial dimensions of the field-of-view of the sensor, and the third representing time. Each bit-plane slice is a single readout field. For single-bit QIS devices, the jot data cube is binary in nature. For multi-bit QIS, the jot data cube consists of words of bit length corresponding the readout quantization bit depth described in more detail below.

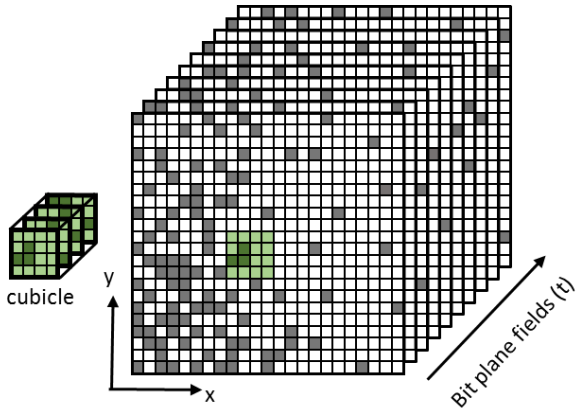

Figure 1. Conceptual illustration of a jot data cube and a 4x4x4 cubicle subset.

In perhaps the simplest form, image pixels can be created from the sum of a small x-y-t "cubicle" of bits from the jot data cube. The dimensions of the cubicle determine the spatial and temporal resolution of the output image, and all jot values within the cubicle are weighted equally. The maximum signal-to-noise ratio (SNR) of the image pixel (assuming an ensemble of pixels created from the same illumination and readout conditions) is determined by the size of the cubicle. For example, a cubicle of size 16x16x16 of single-bit QIS jots summed together would have a maximum value of 4096 and a maximum SNR of $\sqrt{4096} = 64$. Illustration of image formation from jot data is shown in Fig. 2.

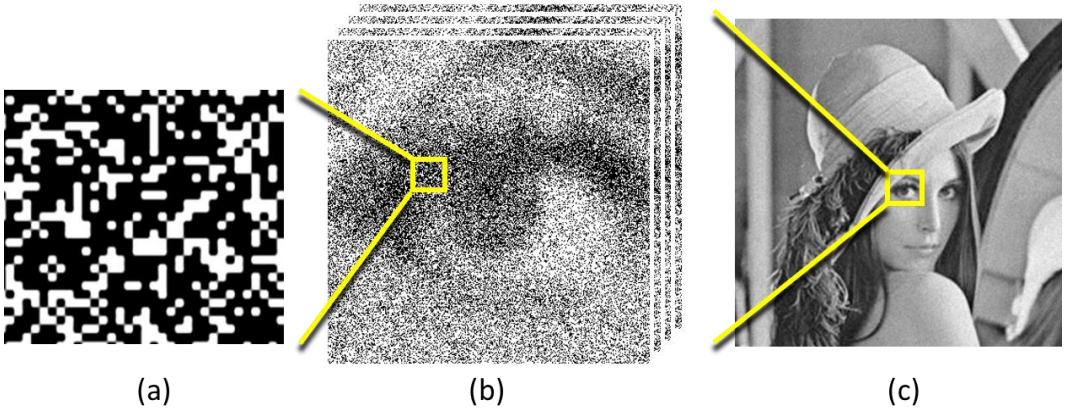

Figure 2. Simulation of (a) raw jot data, (b) same at lower magnification, (c) after processing cubicles to form grey scale image.

3. IMAGING CHARACTERISTICS

3.1. Hurter-Driffield Characteristic Response (D-LogH)

In the QIS, the statistical nature of the arrival of photons and the photoelectrons they produce are well described by Poisson arrival statistics. For convenience we define the quanta exposure *H* as the average number of photoelectrons collected by a jot over an integration period, which depends on factors such as the incident photon flux, effective jot area, quantum efficiency, carrier collection efficiency and integration time. The probability of there being *k* photoelectrons is given by the Poisson mass function:

$$\mathbb{P}[k] = \frac{e^{-H}H^{k}}{k!} \tag{1}$$

The probability that there are no photoelectrons is $\mathbb{P}[0] = e^{-H}$, and the probability of at least one photoelectron is $\mathbb{P}[k > 0] = 1 - \mathbb{P}[0] = 1 - e^{-H}$. In the single-bit QIS, reading out no photoelectrons is a logic "0" and reading out one or more photoelectrons is set as a logic "1." Essentially, the full-well capacity (*FWC*) of the single-bit QIS is 1e-. The bit density *D* of jots (fraction per bit ensemble that have logic value "1") gives rise to an S-shaped curve if *D* is plotted as a function of log(*H*), reflecting the relationship [3,9]:

$$D = 1 - e^{-H} \tag{2a}$$

This characteristic QIS-response curve is shown in Fig. 3a. This behavior is similar to the behavior of an ensemble of avalanche detectors in a Si photomultiplier and also observed in SPADs and in subsequent analysis of binary sensors [31, 28,29]. The standard deviation of *D* (or noise, σ) is given by:

$$\sigma = \sqrt{e^{-H}\left[1 - e^{-H}\right]} \tag{2b}$$

as shown in Fig. 4.

The statistical nature of photoelectron counting (or essentially photon counting if the efficiency factors above are close to unity) is the same as that which gives rise to the *D*-log(*H*) nature of film exposure reported by Hurter and Driffield in 1890 [30] due to the statistical exposure of film grains, as shown in Fig. 3b. The curve shape is determined by the underlying statistical physics of exposure and threshold for creating jots with value "1," and is not influenced strongly by circuit or device performance.

3.2 Flux Capacity

An important figure of merit for QIS devices is flux capacity. Flux capacity ϕ_w is defined as the nominal maximum photon flux that results in *H*=1. It is dependent on the density of jots j in the image sensor (jots/cm^2), the readout field rate f_r, the shutter duty cycle δ and the effective quantum efficiency $\bar{\gamma}$ according to [14]:

$$\phi_w = jf_r/\delta\bar{\gamma} \tag{3}$$

For photography and cinematography, high flux capacity is required so that the QIS does not saturate under normal imaging conditions. Note that in fact the QIS can handle exposures for *H*>1 without saturating, typically 5x higher due to its overexposure latitude, but *H*=1 is taken for convenience. It can be seen that high jot density and high field readout rate are driven by flux capacity and not necessarily by improved spatial or temporal resolution of the final image, although these are additional benefits. The sub-diffraction jot pitch requires use of advanced-node processes that are expensive and difficult to access today. The high readout rate creates challenges in controlling power dissipation in the readout circuit.

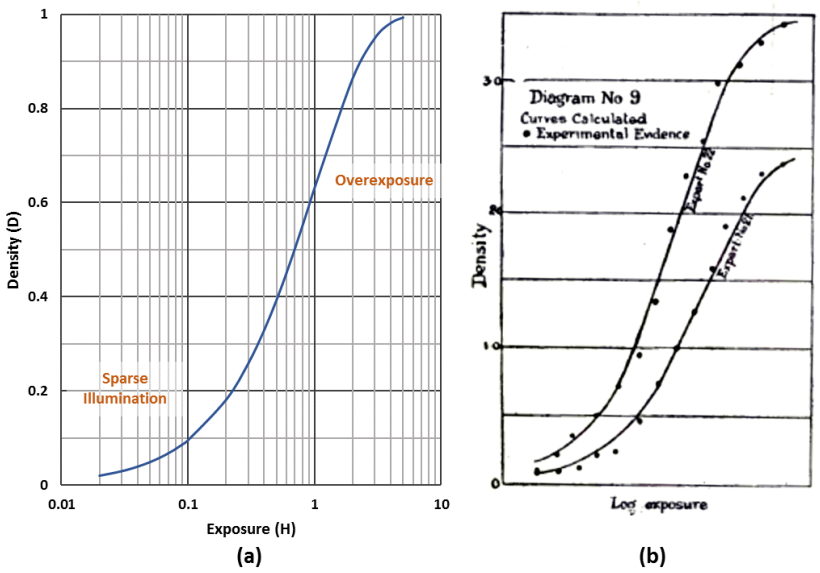

Figure 3. (a) Single-bit QIS bit density as a function of quanta exposure, in D-log(H) format. Sparse and over exposure regions are labelled [9]. (b) D-log(H) curve for photographic plates as reported by Hurter and Driffield in 1890 [30].

3.3 Multi-bit QIS

To further improve flux capacity, the multi-bit QIS was proposed. In the multi-bit QIS, the readout result can result in 2^n states, where n is the readout bit depth, typically $1 \leq n \leq 5$ and FWC of $2^n - 1$. (A single-bit QIS is, in essence, a special case of a multi-bit QIS with n=1.) The flux capacity ϕ_{wn} is increased to:

$$\phi_{wn} = jf_r(2^n - 1)/\delta\bar{\gamma} \tag{4}$$

The Hurter-Driffield response is modified by multi-bit QIS readout resulting in higher saturation signal, less non-linearity and less overexposure latitude [9,14].

Consider an ensemble of 4096 jots. For a single-bit QIS, the maximum signal obtained by adding together the logical readout signal from each jot (0 or 1) is 4096. For the 2-bit QIS, the maximum signal is increased by three-fold $(2^n - 1)$ to 12,288 and the noise characteristic rolls off more steeply. The summed signal of an ensemble of 4096 multi-bit jots is shown in Fig. 4.

3.4 Signal-to-Noise Ratio (SNR) and Dynamic Range (DR)

The use of exposure-referred SNR (SNR_H) is useful for non-linear devices, especially when noise drops near saturation. The SNR_H for normal readout of a single-bit QIS is given by [9]:

$$SNR_H = \sqrt{M}\frac{H}{\sqrt{e^H - 1}} \tag{5}$$

where M is the number of jots in the ensemble or cubicle used for the read signal sum. For normal readout, the SNR_H reaches a maximum value at $H \cong 1.6$ and the maximum value of SNR_H is approximately $0.8\sqrt{M}$. For multi-bit QIS, maximum SNR_H grows as ~ $\sqrt{FWC}$.

Dynamic range (DR) for the QIS is defined as the range between low signal H_{min} where SNR_H =1 (essentially where the ensemble of read out jots has a total sum of one photoelectron) and high signal H_{max} where SNR_H drops back down to unity (and lower) due to saturation [9]. The DR depends on the size of the ensemble – more jots, higher dynamic range, and the DR scales approximately as M.

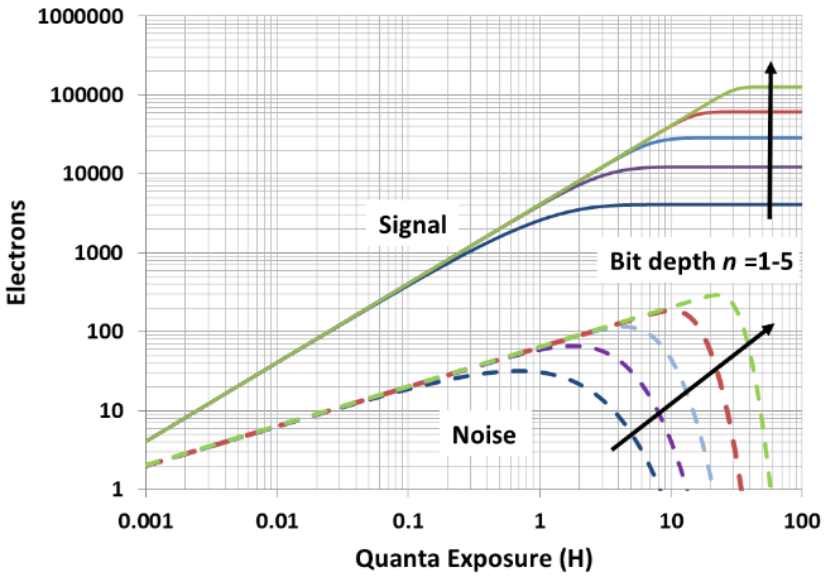

Figure 4. Log signal and noise as a function of log exposure for multi-bit QIS jots with varying bit depth. The signal is the expected sum over 4096 jots (e.g. 16x16x16). Saturation signal is $4096 \cdot (2^n - 1)$. (From [14])

3.5 High Dynamic Range (HDR)

Since the QIS consists of multiple fields of jot data that may be combined in a cubicle ensemble, it is possible to have a different electronic shutter duty cycle or "speed" for each field or time slice. Thus some time slices can have high flux capacities allowing capture of brighter portions of scenes without saturation. A similar idea has been used in CMOS image sensors for many years [35] for high dynamic range (HDR) imaging, although it can suffer from imaging artifacts due to relative motion of the scene between captured fields. The higher field readout rate of the QIS will ameliorate some of those artifacts. The Hurter-Driffield response characteristics of the QIS help reduce SNR "dips" caused by the fusion of multiple fields of data taken with different shutter speeds [9]. Multi-bit QIS devices can also be operated in HDR mode. For example, consider 2b-QIS output formed from a 16x16x16 cubicle. In an HDR mode, with summing a cubicle where 13 fields are exposed with 100% shutter duty cycle, 1 field at 20% duty cycle, 1 field at 4% duty cycle, and 1 field at 0.8% duty cycle, the dynamic is extended to approximately 135dB as illustrated in Fig. 5.

4. READ NOISE AND COUNTING ERROR RATES

4.1 Read Noise and Readout Signal Probability

Counting photon or photoelectrons requires deep sub-electron read noise (DSERN), that is, read noise less than 0.50e- rms. It has been suggested that 0.3e- rms read noise is sufficient for many photon-counting applications [36,32,37] however accurate counting with low error rate under low exposures (e.g. H<0.2) requires read noise less than 0.15e- rms [21].

When both read noise and conversion gain variation is considered for an ensemble of jots that are read out, the probability distribution of readout voltages is given by:

$$P[U] = \sum_{k=0}^{\infty} \frac{\mathbb{P}[k]}{\sqrt{2\pi\sigma_k^2}} exp\left[-\frac{(U-k)^2}{2\sigma_k^2}\right] \tag{6}$$

where U is the readout signal normalized by mean conversion gain (in electron number), u_n is the read noise (in e- rms), and where σ_k is given by:

$$\sigma_k \triangleq \sqrt{u_n^2 + (k\sigma_{CG}/\overline{CG})^2} \tag{7}$$

and σ_{CG} is the standard deviation of conversion gain in the ensemble, and $\overline{CG}$ is the mean conversion gain in the ensemble.

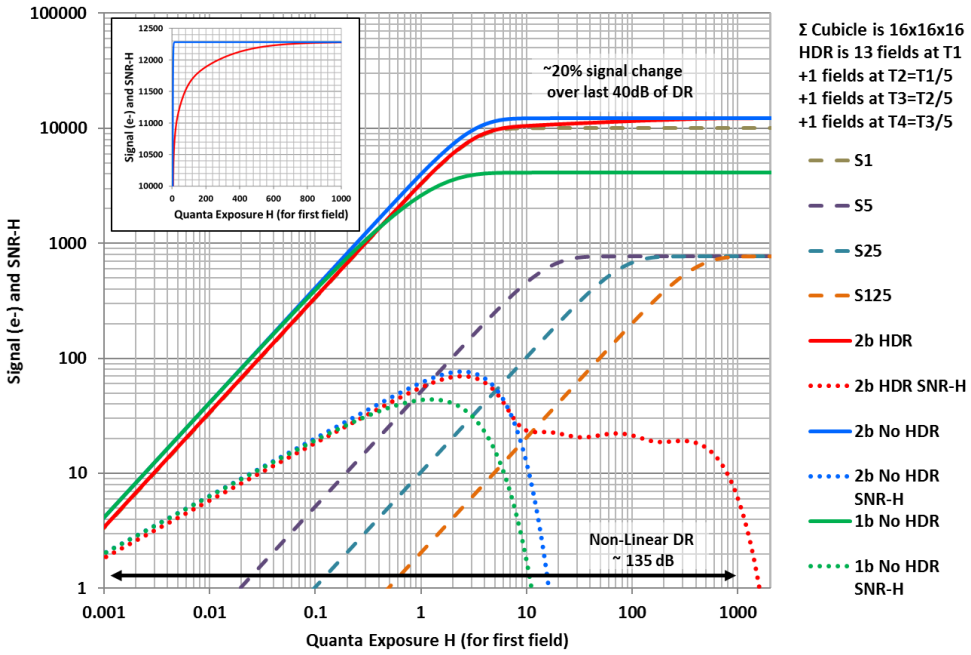

Figure 5. Log signal vs. log exposure for a 2b QIS operated in normal readout mode (blue) and high dynamic range mode (red), showing extension of the dynamic range by approximately 40 dB. Inset shows linear-scale response curves for the extended exposure range.

4.2 Quantization and Bin Counts

In a single-bit QIS, the threshold level U_{T1} for setting the output to a logic "1" is U_{T1}=0.5, so that the digital output is "1" for U>0.5 and otherwise "0". For multi-bit QIS, additional thresholds are set at integer increments above U_{T1} (e.g. U_{T2}=1.5, U_{T3}=2.5 etc.). All read out signals lying between two adjacent thresholds (a bin) result in the count for that bin C_N being incremented by one. False positive counts are generated when a read out signal is misquantized into the wrong bin due to noise and conversion gain variation. These false positives (and their corresponding false negatives) give rise to an error in the total count.

An ensemble of M jots results in a total of M counts spread across the 2^n bins of a multi-bit QIS. As shown in Fig. 6, the total count in each bin can be used to determine the expected total number of photoelectrons collected by the ensemble N_{TOT} such that [21]:

$$N_{TOT} = M \sum_{N=0}^{\infty} N \cdot C_N \tag{8}$$

For $\sigma_k \lesssim$0.50e- rms, the expected count in each bin for a single jot is given by:

$$C_N \cong \sum_{k=N-1}^{N+1} \frac{1}{2} \mathbb{P}[k] \left[\mathrm{erf}\left(\frac{N+\frac{1}{2}-k}{\sigma_k \sqrt{2}} \right) - \mathrm{erf}\left(\frac{N-\frac{1}{2}-k}{\sigma_k \sqrt{2}} \right) \right] \tag{9}$$

The expected count in Eq. 8 can be used to estimate the count for an ensemble of M jots. For example, consider a single-bit QIS array of jots with pitch of 1μm. An ensemble of 100 jots, formed from 10x10x1 cubicle would cover an area of size 10μmx10μm. For a quanta exposure H=0.01, the ideal count from the ensemble would by $N_{TOT} = 1$. Using Eqs. 8-9,

or Fig. 6, one obtains an expected count of 1.04e- for a jot read noise of 0.15e- rms, but 5.68e- for a read noise of 0.3e- rms (assuming no dark counts).

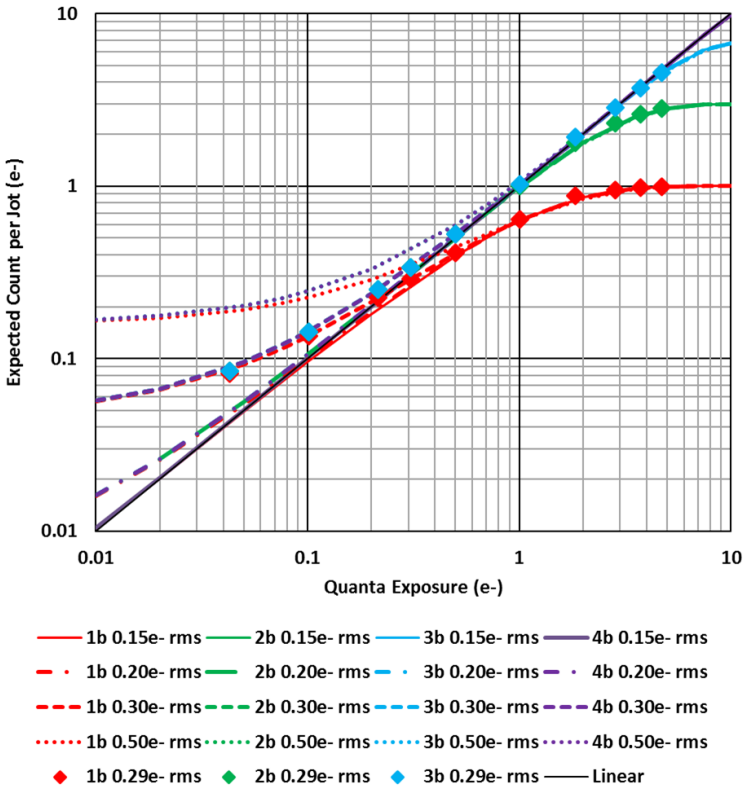

Figure 6. Expected count vs. quanta exposure for various bit depths and read noise levels. Experimental data is shown by the diamond symbols [after 21].

5. JOT DEVICE

5.1. Background and Motivation

The ultimate goals of a jot device include small pitch size (200nm-500nm), low read noise (<0.15e- rms), low dark current (<1e-/s), small FWC (1-100e-) and strong compatibility with a CIS fabrication line. One big difference between a jot and a conventional CIS pixel is its deep sub-electron read noise and photoelectron counting capability. A conventional CIS usually has voltage read noise higher than 100μV rms and CG lower than 100μV/e-, yielding read noise higher than 1e- rms. Higher CG and lower voltage noise reduce input-referred read noise.

Our approach to achieve deep sub-electron read noise is to improve CG and reduce SF transistor noise. Since our first report of success with this approach [14, 17] other groups have also reported success at achieving deep sub-electron read noise (and photon counting) without the use of avalanche gain [33,34]. Improvement of CG was also reported in [38] leading to 0.46e- rms read noise, just short of what is needed to demonstrate photoelectron counting.

The photoelectron signal is converted to a voltage signal for readout using the capacitance of the floating diffusion (FD) node. The voltage signal generated by one photoelectron is given by,

$$CG = \frac{q}{C_{FD}}, \tag{10}$$

where q is the elementary charge of one electron and C_{FD} is the node capacitance of FD that includes several major components: depletion capacitance between FD and substrate, overlap capacitance between FD and the transfer gate (TG), overlap capacitance between FD and reset gate (RG), SF effective gate capacitance, and inter-metal capacitance. To improve CG, the capacitance of FD needs to be reduced. Note that the reduction of FD capacitance may lead to reduction of FWC in conventional CIS, but it is not a concern for a jot device as the required FWC is very small.

5.2. High CG Pump-gate Jot Devices

Depending on the process feature size and layout design, the overlap capacitance between FD and TG in a CIS pixel can be 0.3fF or higher, especially in a pixel with a shared readout structure. The pump-gate (PG) technique was developed by our group to eliminate the overlap capacitance between FD and TG without affecting complete charge transfer [13] as illustrated in Fig. 7.

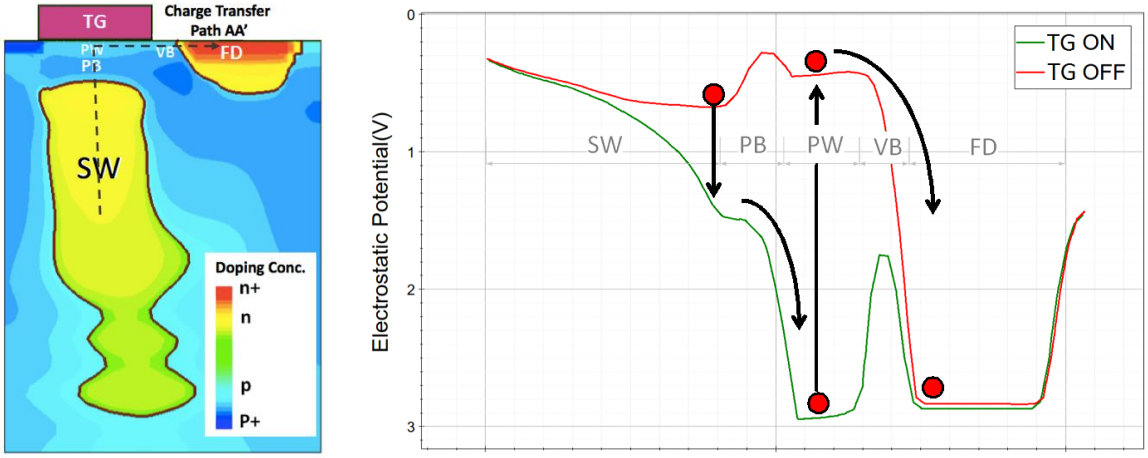

(**a**) (**b**)

Figure 7. (a) PG jot cross-section doping profile from TCAD simulation. (b) Electrostatic potential curve along charge transfer path AA'. Both are presented in [13].

A tapered RG technique was developed to reduce the overlap capacitance between FD and RG, which uses STI to shrink the width of reset transistor on the FD end. The use of the tapered RG (aka tapered PG (TPG) jot) significant increased conversion gain from 250uV/e- to over 400uV/e- and helped reduce read noise from approximately 0.33-0.45e- rms range to the 0.22-.35e- rms range [18].

The pump-gate technique enables the implementation of shared readout structure (shared PG jot) without adding overlap capacitance due to the distal FD, and the 3D TCAD model of a 4-way shared readout PG jot is depicted in Fig. 8. The shared readout jot has a more compact layout design with 1μm pitch, but since FD needs to be connected to the SF, more inter-metal parasitic capacitance is added to FD, which yields a mildly lower CG.

All jots were designed and fabricated in the TSMC BSI 65nm process. The fabrication followed baseline process with implantation modifications, and no extra mask was required. The TPG jot pitch is 1.4μm and has 410μV/e- CG (0.39fF FD capacitance), the non-shared PG jot pitch is 1.4μm and has 250μV/e- CG (0.64fF FD capacitance), and the 4-way shared PG jot pitch is 1μm and has 230μV/e- CG (0.7fF FD capacitance). As expected, extremely low SW dark current (0.1e-/s at RT) was measured and almost lag-less (<0.1e-) charge transfer was achieved. The measured characteristics of jot devices are listed in Table 1.

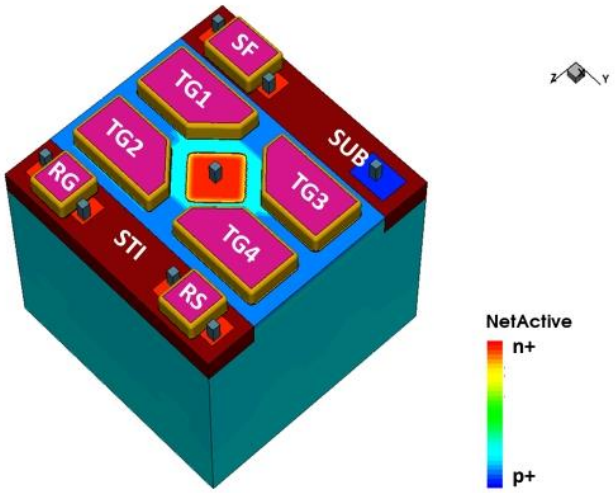

Figure 8. TCAD 3D model of a 4-way shared readout jot, from [20].

Table 1. Summary of characterization results of PG jot devices

Quantity	TPG jot	Non-shared PG jot	Shared PG jot
CG	410μV/e-	250μV/e-	230μV/e-
Read Noise	0.29e- rms (129μV rms)	0.38e- rms (95.3μV rms)	0.48e- rms (110μV rms)
SF Size	0.2x0.2μm²	0.2x0.4μm²	0.2x0.4μm²
Dark Current @ RT	0.09e-/s (0.73pA/cm²)	0.12e-/s (0.98pA/cm²)	Not measured
Dark Current @ 60℃	1.29e-/s (10.5pA/cm²)	1.26e-/s (10.2pA/cm²)	0.71e-/s (11.4pA/cm²)
Lag @ RT	<0.1e-	<0.1e-	<0.12e-

5.3. Photoelectron Counting Capability

Both the PG and TPG jots are demonstrated to have deep sub-electron read noise, and the PCH-VPM method was used to characterize their photoelectron counting capability [17,18]. The jots in each 32x32 array were readout by single CDS under room temperature (RT). TPG jots have an average read noise of 0.29e- rms, or 129μV rms voltage noise, and a "golden" TPG jot achieved 0.22e- rms read noise. The PCH of the "golden" TPG jot is depicted in Fig. 9a. It was the first time that a CIS pixel without avalanche gain achieved deep sub-electron read noise and photoelectron counting capability. PG jots have an average read noise of 0.38e- rms, or 95.3μV rms voltage noise. Shared readout PG jots have an average read noise of 0.48e- rms, or 110μV rms voltage noise [20]. The PCHs of these jots are also shown in Figs. 9b and 9c.

6. LOW POWER AND HIGH SPEED READOUT CIRCUITS

The principal challenge addressed in this section is the design of internal high-speed and low-power addressing and readout circuitry for the QIS. A QIS may contain over a billion jots, each producing just 1mV/e- of signal, with a field readout rate 10-100 times faster than conventional CMOS image sensors.

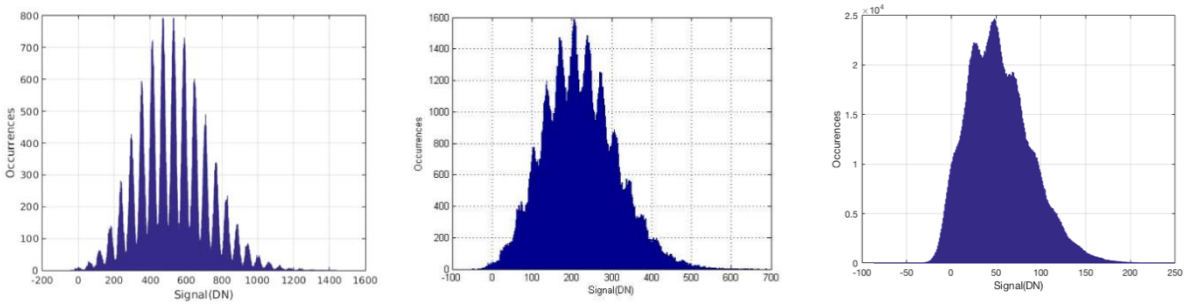

(**a**) (**b**) (c)

Figure 9. (a) PCH of a "golden" TPG jot with 0.22e- rms read noise for a quanta exposure of 9. Presented in [18]. (b) PCH of a PG jot with 0.32e- rms for a quanta exposure of 6.5. Presented in [17]. (c) PCH of a shared readout PG jot with 0.42e- rms read noise for a quanta exposure of 2.4. Presented in [20].

6.1. Readout Circuits for Single-bit QIS

To implement the single-bit QIS ADC, the inherent random offset in a comparator and latch circuit must be overcome to permit practical use of a 500uV comparator threshold voltage. This traditionally requires additional gain and concomitant power dissipation. For low power, a charge-transfer amplifier (CTA) approach was taken [10]. Minimizing the power dissipation was achieved by using a 4-stage charge-transfer amplifier (CTA) as a gain stage in the analog readout signal chain. Use of CTA technique implemented in pathfinder test chips have resulted in a significant improvement in an energy-per-bit figure of merit (FOM) compared to previous work, although detailed comparison is complicated.

In the first test chip, low-power readout circuits based on the CTA were implemented in a 1000fps megapixel binary imager [15,19]. The 1376(H)x768(V) pixel image sensor uses a partially- pinned photodiode, 3.6µm 3T pixel, and readout architecture implemented in the X-FAB 0.18µm process. The sensor is operated in a single-row rolling-shutter mode so true correlated double sampling (CDS) can be utilized. This means that when a particular row is accessed, it is first reset, allowed to briefly integrate a signal, and then read out before moving to the next row. However, to achieve 1000fps, this leads to extremely short integration times (i.e. <1 µs), useful only in the lab. To characterize the pixels, lower frame rates were used.

A column-parallel single-bit ADC using a CTA-based design detects a minimum 0.5mV output swing from the pixel. The ADC is capable of sampling at speeds of 768kSa/s. The sensor operates at 1000fps, which corresponds to a row time of 1.3µs, a signal integration time, Tint, of 0.9µs, and an output data rate of 1Gb/s.

The final specifications of the image sensor are shown in Table 2. The power consumption of the entire chip (including I/O pads) is 20mW. Total power consumption of the ADCs is 2.6mW which corresponds to 1.9µW per column. The row addressing circuits including the buffers consume 0.73µW per row, whereas the column shift registers dissipate 2.3µW per column. The ADCs working in tandem with digital circuits consume an average power of 6.4mW. It is also noted that in the QIS, input offset at 3σ must be less than $1/2V_{LSB}$ (=0.5mV for this chip) which requires additional power dissipation. The FOM of the pathfinder chip is 2.5pJ/b.

The second test sensor explores the low-power readout circuits needed for a 1040fps gigapixel binary image sensor [23,25]. Due to limited available area on the die, only 32 of the columns (12,000 pixels in each column) and 16 1b-ADCs were implemented in this test chip. Since the column parallel architecture is used, the power consumption of a column can be multiplied by 2x42,000 to estimate the expected total power consumption of a gigajot QIS. This imager was implemented in a 65nm BSI CMOS process. Pixel pitch is 1.4µm pitch, and 4-way-shared PPD pixels are used in the imager. The same structures of the sense-amplifier and 1b-ADC (size of the transistors and capacitors are scaled down) are implemented in this test chip.

Table 2. Specifications of the 1MP binary image sensor.

Process		X-FAB, 0.18 μm, 6M1P (non-standard implants)
VDD		1.3 V (Analog and Digital), 1.8 V (Array), 3 V (I/O pads)
Pixel type		3T-APS
Pixel pitch		3.6 μm
Photo-detector		Partially pinned photodiode
Conversion gain		119 μV/e-
Array		1376 (H) X 768 (V)
Column noise		2 e-
Field rate		1000 fps
ADC sampling rate		768 KSa/s
ADC resolution		1 bit (VLSB = 1 mV)
Output data rate		32 (output pins) X 33 Mb/s = 1 Gb/s
Package		PGA with 256 pins
Power	**Pixel array**	8.6 mW
	ADCs	2.6 mW
	Addressing	3.8 mW
	I/O pads	5 mW
	Total	20 mW

The average power consumption per column (biasing a column with 24,000 pixels and a sense-amplifier and a 1b-ADC) is 68uW. It is estimated that the power consumption of a gigapixel QIS imager, (ADCs and column biasing) would be approximately 2.85W. The FOM of the sense-amplifiers and ADC is 0.4pJ/b. Comparing the power consumption of the ADC that is used in the first single-bit chip (FOM = 2.5pJ/b) with the ADC in this work, shows that using more advanced technology node (65nm in this work and 0.18μm in the first test chip) yields 6x improvement in FOM.

6.2. Readout Circuits for multi-bit QIS

Conceptually, once input-referred read noise is low enough to count a single photoelectron reliably, counting multiple photoelectrons with the same photodetector and readout structure and a low-bit-depth ADC also becomes practical, allowing implementation of a multi-bit QIS. The ADC digital value is the number of photoelectrons in the jot.

Increasing the bit depth of a jot from single-bit to *n* bits allows the field readout rate to be reduced while maintaining constant flux capacity. Thus, while ADC energy per readout is increased by increasing the jot bit depth, the power dissipation increase is mitigated or negated by the reduced field readout rate. The multi-bit QIS approach also addresses the column limited bandwidth issue, where in single-bit QIS imager, since the integration time is shorter than the integration time in multi-bit QIS, imaging throughput is limited. We have explored several variations of multi-bit QIS architectures, including single-slope, cyclic, and successive approximation ADCs implemented in 180nm CIS process [14]. Results are promising and will be reported in a future publication.

7. CONCLUSIONS

This paper has presented a review of progress to date on the Quanta Image Sensor made by the group at Dartmouth and others, as well as a brief review of related activity. Much progress has been made since 2012 when work started in earnest at Dartmouth. Implementation of all the critical elements of the QIS has been demonstrated, including image formation, photon-counting jots, and low-power readout electronics. Demonstration of megajot QIS arrays is possible over the next year or two.

ACKNOWLEDGMENTS

This work was sponsored in part by Rambus, Inc. The authors appreciate discussion with the students and faculty at Dartmouth as well as with visiting scientists and colleagues in academic and industry, including Forza Silicon, TSMC, XFAB and Rambus. In particular, we would like to thank Prof. Kofi Odame at Dartmouth, Dr. Barmak Mansoorian at Forza Silicon, and Jay Endsley and Michael Guidash at Rambus Inc. We would also like to especially thank graduate students Leo Anzagira, Song Chen, Donald Hondongwa, Arun Rao, Yue Song, and Dakota Starkey, and Rachel Zizza for their contributions.

REFERENCES

1. E.R. Fossum, “Image sensor using single photon jots and processor to create pixels,” US Patent No. 8,648,287.
2. E.R. Fossum, “Some Thoughts on Future Digital Still Cameras,” pp. 305-314 in Image Sensors and Signal Processing for Digital Still Cameras, J. Nakamura, ed., CRC Titles Press, 2005. ISBN: 0849335450
3. E.R. Fossum, “What to do with sub-diffraction-limit (SDL) pixels? – A proposal for a gigapixel digital film sensor (DFS),” in Proc. of the 2005 IEEE Workshop on Charge-Coupled Devices and Advanced Image Sensors, Karuizawa, Japan, June 2005.
4. E.R. Fossum, “Gigapixel digital film sensor,” in Nanospace Manipulation of Photons and Electrons for Nanovision Systems, The 7th Takayanagi Kenjiro Memorial Symposium and the 2nd Intl. Symposium on Nanovision Science, Univ. of Shizuoka, Hamamatsu, Japan, October 25-26, 2005.
5. E.R. Fossum, D-K. Cha, Y-G. Jin, Y-D. Park, S-J. Hwang, “High sensitivity image sensors including a single electron field effect transistor and methods of operating the same,” US Patent No. 8,546,901 and 8,803,273.
6. E. Fossum, "The Quanta Image Sensor (QIS): concepts and challenges," in Imaging and Applied Optics, OSA Technical Digest (CD) (Optical Society of America, 2011), paper JTuE1. doi:10.1364/COSI.2011.JTuE1
7. S. Chen, A. Ceballos, and E.R. Fossum, “Digital integration sensor,” in Proceedings of the 2013 Int. Image Sensor Workshop, Snowbird, Utah USA June 12-16, 2013.
8. D. Hondongwa, J. Ma, S. Masoodian, Y. Song, K. Odame and E.R. Fossum, “Quanta Image Sensor (QIS): early research progress,” In Applied Industrial Optics: Spectroscopy, Imaging and Metrology, pp. JW3B-2. In Proc. 2013 Opt. Soc. Am. Topical Meeting on Imaging Systems, Arlington, VA USA June 24-27, 2013. doi:10.1364/AIO.2013.JW3B.2
9. E.R. Fossum, “Modeling the performance of single-bit and multi-bit quanta image sensors,” IEEE J. Electron Devices Society, vol.1, no. 9, pp. 166-174 September 2013.
10. S. Masoodian, K. Odame, and E.R. Fossum, “Low-power readout circuit for quanta image sensors,” Electronics Letters, vol. 50, no. 8, pp. 589–591, April 2014.
11. J. Ma, D. Hondongwa, and E.R. Fossum, “Jot devices and the quanta image sensor,” in Technical Digest of the 2014 IEEE International Electron Devices Meeting (IEDM), pp. 247-250, San Francisco, CA December 2014.
12. L. Anzagira and E.R. Fossum, Color filter array patterns for small-pixel image sensors with substantial cross talk, J. Opt. Soc. Am. A, vol. 32, no. 1, pp. 28-34, January 2015.
13. J. Ma and E.R. Fossum, “A pump-gate jot device with high conversion gain for quanta image sensors,” IEEE J. Electron Devices Society, vol. 3, no. 2, pp. 73-77, March 2015.
14. E.R. Fossum, “Multi-bit quanta image sensors,” in Proc. 2015 Int. Image Sensor Workshop (IISW), June 8-11, Vaals, Netherlands 2015. in Proc. 2015 Int. Image Sensor Workshop (IISW), June 8-12, Vaals, Netherlands 2015.. and slides: http://imagesensors.org/wp-content/uploads/2016/03/2015-June-IISW-Multibit-QIS.pdf

15. S. Masoodian, A. Rao, J. Ma, K. Odame and E.R. Fossum, A 2.5pJ Readout Circuit for 1000fps Single-Bit Quanta Image Sensors, in Proc. 2015 Int. Image Sensor Workshop (IISW), June 8-11, Vaals, Netherlands 2015. and slides: http://imagesensors.org/wp-content/uploads/2016/03/2015-IISW-Masoodian-Mpixel-binary-sensor.pdf
16. R. Zizza, Jots to Pixels: Image Formation Options for the Quanta Image Sensor, M.S. Dissertation Thesis, Thayer School of Engineering at Dartmouth College, July 2015.
17. J. Ma and E.R. Fossum, "Quanta image sensor jot with sub 0.3e- rms read noise and photon counting capability," IEEE Electron Device Letters, vol. 36, no. 9, pp. 926-928, September 2015.
18. J. Ma, D. Starkey, A. Rao, K. Odame, and E.R. Fossum, "Characterization of quanta image sensor pump-gate jots with deep sub-electron read noise," IEEE J. Electron Devices Society, vol. 3, no. 6, pp. 472-480, November 2015.
19. S. Masoodian, A. Rao, J. Ma, K. Odame and E.R. Fossum, "A 2.5pJ/b binary image sensor as a pathfinder for quanta image sensors," IEEE Trans. Electron Devices, vol. 63, vol. 1, pp. 100-105, January 2016.
20. J. Ma, L. Anzagira, and E.R. Fossum, "A 1μm-pitch quanta image sensor jot device with shared readout," IEEE J. Electron Devices Society, vol. 4, no. 2, pp. 83-89, March 2016.
21. E.R. Fossum, "Photon counting error rates in single-bit and multi-bit quanta image sensors," IEEE J. Electron Devices Society, vol. 4, no. 3, pp. 136-143, May 2016. doi:10.1109/JEDS.2016.2536722
22. D.A. Starkey and E.R. Fossum, "Determining conversion gain and read noise using a photon-counting histogram method for deep sub-electron read noise image sensors," IEEE J. Electron Devices Society, vol. 4, no. 3, pp. 129-135, May 2016.. doi:10.1109/JEDS.2016.2536719
23. E.R. Fossum, "Photon counting without avalanche multiplication - progress on the quanta image sensor," in Proc. Image Sensors 2016 Europe, 15-17 March 2016 – Park Plaza, London UK. Available at smithersapex.com. Retrieved from: http://ericfossum.com/Presentations/2016%20March%20QIS%20London.pdf
24. L. Anzagira and E.R. Fossum, "Application of the quanta image sensor concept to linear polarization imaging – a theoretical study," accepted April 2016 for future publication in J. Opt. Soc. Am. A.
25. S. Masoodian and E.R. Fossum, "A 32 x 12000, 1040fp/s binary image sensor with 0.4pj/b readout circuits fabricated in 65nm backside-illuminated CIS process as a path-finder for 1Gpixel 1040fps binary image sensor," submitted March 2016 to IEEE J. Solid-State Circuits.
26. J. Ma and E.R. Fossum, "TCAD simulation of a quanta image sensor jot device with a JFET source follower," to be submitted April 2016 to IEEE J. Electron Devices Soc.
27. E.R. Fossum, J. Ma, S. Masoodian, L. Anzagira, and R. Zizza, "Quanta image sensor: every photon counts." to be published in MDPI Sensors, Special Issue on Photon-Counting Image Sensors, 2016.
28. L. Sbaiz, F. Yang, E. Charbon, S. Süsstrunk, and M. Vetterli. "The gigavision camera." In Acoustics, Speech and Signal Processing, ICASSP 2009 doi:10.1109/ICASSP.2009.4959778.
29. F. Yang, L. Sbaiz, E. Charbon, S. Süsstrunk, and M. Vetterli. "On pixel detection threshold in the gigavision camera." In IS&T/SPIE Electronic Imaging, pp. 75370G-75370G. International Society for Optics and Photonics, 2010. doi:10.1117/12.840015
30. F. Hurter and V.C. Driffield, "Photo-chemical investigations and a new method of determination of the sensitiveness of photographic plates," J. Soc. Chemical Industry, vol. IX, no. 5, pp. 31st May 1890, as reprinted in The Photographic Researches of Ferdinand Hurter and Vero C. Driffield, W.B. Ferguson, Ed., published by the Royal Photographic Society of Great Britain, 35, Russel Square, W.C., London, England, 1920, pp. 76-122. Retrieved from: https://archive.org/details/memorialvolumeco00hurtiala
31. G. Bondarenko, B. Dolgoshein, V. Golovin, A. Ilyin, R. Klanner, and E. Popova. "Limited Geiger-mode silicon photodiode with very high gain." Nuclear Physics B-Proceedings Supplements vol. 61, no. 3, pp. 347-352, 1998.
32. Q. Yao, B. Dierickx, B. Dupont, "CMOS image sensor reaching 0.34e- r.m.s. read noise by inversion-accumulation cycling," in Proc. 2015 Int. Image Sensor Workshop (IISW), June 8-11, Vaals, Netherlands 2015.
33. J. Janesick, T. Elliott, J. Andrews, and J. Tower, "Fundamental performance differences of CMOS and CCD imagers: Part VI," in Proc. SPIE, vol. 9591. Target Diagnostics Physics and Engineering for Inertial Confinement Fusion IV, 959102 San Diego, CA 31 August 2015. doi:10.1117/12.2189941
34. M-W Seo, et al., "A 0.27e− rms read noise 220-μV/e− conversion gain reset-gate-less CMOS image sensor with 0.11-μm CIS process," IEEE Electron Device Letters, vol. 36, no. 12, pp. 1344-1347, Dec. 2015.
35. O. Yadid-Pecht, C. Staller, and E.R. Fossum, "Wide intrascene dynamic range CMOS APS using dual sampling," IEEE Trans. Electron Devices, vol. 44, no. 10, pp. 1721-1723 October 1997.
36. N. Teranishi, "Required Conditions for Photon-Counting Image Sensors," IEEE Trans. Electron Devices, vol. 59, no. 8, pp. 2199-2205, Aug. 2012.

37. A. Boukhayma, A. Peizerat, and C. Enz, “Noise reduction techniques and scaling effects towards photon counting CMOS image sensors,” MDPI Sensors, vol. 16, no. 4, p. 514, 2016.
38. F. Kusuhara, S. Wakashima, S. Nasuno, R. Kuroda and S. Sugawa, “Analysis and reduction of floating diffusion capacitance components of CMOS image sensor for photon-countable sensitivity,” in Proc. 2015 Int. Image Sensor Workshop (IISW), June 8-11, Vaals, Netherlands 2015.